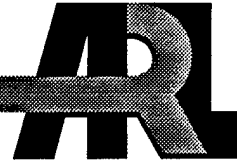


ARMY RESEARCH LABORATORY



Magnetic Induction Launcher Models

by Paul R. Berning
and Charles R. Hummer

ARL-TR-1384

June 1997

BTIC QUALITY INSPECTED 4

Approved for public release; distribution is unlimited.

19970919 027

The findings in this report are not to be construed as an official Department of the Army position unless so designated by other authorized documents.

Citation of manufacturer's or trade names does not constitute an official endorsement or approval of the use thereof.

Destroy this report when it is no longer need. Do not return it to the originator.

Army Research Laboratory

Aberdeen Proving Ground, MD 21005-5066

ARL-TR-1384

June 1997

Magnetic Induction Launcher Models

Paul R. Berning, Charles R. Hummer
Weapons and Materials Research Directorate, ARL

Approved for public release; distribution is unlimited.

Abstract

Various computer models developed to aid in the design of magnetic induction launchers or coilguns are described. The first models the launch process based on launcher circuit parameters, in particular, the coil inductance as a function of projectile position $L(x)$. The second set of models calculates the overall inductance of the launcher coil both with and without the plate present. The difference between the values $\Delta L = L(\infty) - L(0)$ has proven to be a key parameter in determining the relative performance of different launcher designs. The third set of models estimate the fields and forces generated by the launcher, under the assumption of filamentary conductor structures and static conditions. The methods used to avoid the complications associated with the dynamic nature of the actual launch process are described. These last models yield an inductance gradient function dL/dx that is crucial for the assessment of launcher performance. The usefulness of these models has been demonstrated in a project to design a coilgun that launches metal plates against incoming kinetic energy (KE) penetrators.

Acknowledgments

The authors would like to thank Dr. Andrus Niiler and Dr. Clinton Hollandsworth for many useful discussions relating to launcher design. Mr. Alexander Zielinski is thanked for his careful review of this manuscript, and also, Mr. Keith Mahan for aiding in the construction of many of the devices described in this manuscript.

INTENTIONALLY LEFT BLANK.

Table of Contents

	<u>Page</u>
Acknowledgments	iii
List of Figures	vii
List of Tables	vii
1. Introduction	1
2. Modeling EM Plate Launchers	1
2.1 Plate Launch Mechanics	3
2.2 Inductance Calculations	8
2.2.1 <i>Calculating Self-Inductance With No Plate Present</i>	9
2.2.2 <i>Calculating Mutual Inductance With No Plate Present</i>	10
2.2.3 <i>Results</i>	12
2.2.4 <i>Calculating Inductances With a Plate Present</i>	12
2.3 Quasi-Static Model	13
2.3.1 <i>Magnetic Field and Lorentz Force Calculations</i>	13
2.3.2 <i>Plate Models and Inductance Gradient Calculations</i>	15
2.3.3 <i>Magnetic Field Results</i>	20
2.3.4 <i>Intracoil Stresses</i>	21
3. Conclusion	23
4. References	25
Distribution List	27
Report Documentation Page	31

INTENTIONALLY LEFT BLANK.

List of Figures

<u>Figure</u>		<u>Page</u>
1.	Inductance and Inductance Gradient vs. Plate Position for Two Different Coil Designs	5
2.	A Typical Fit of Plate Launch Model Results to Measured Current Data	6
3.	Theoretical Final Plate Velocities vs. Initial Voltage for Two Different Coil Designs	7
4.	Filamentary Structures Used to Model a Square Plate and Square Pancake Coil System	18
5.	Measured Inductance Gradient of a 6-in Square Pancake Coil Compared to the Results of Simulations Performed with the Program BFIELD10	18
6.	Measured Inductance Gradient of a 10-in \times 6-in Rectangular Pancake Coil Model Compared to the Results of Simulations	19
7.	The Test Stand Used in a Study of the EM Fields Generated by an Induction Launcher	20
8.	The Magnitude of the Measured Magnetic Field Compared to Simulations	22
9.	Calculated Forces on One Section of a Square Pancake Coil	22

List of Tables

<u>Table</u>		<u>Page</u>
1.	A Comparison of Predicted vs. Actual Final Velocities for Three Shots of the Box Coil	7
2.	A Comparison of Four Different Launcher Designs Based on Simulations	8

INTENTIONALLY LEFT BLANK.

1. Introduction

The work reported here is an outgrowth of a program to develop a system that can aid in the protection of vehicles from long-rod kinetic energy (KE) projectiles. In the past, there have been investigations into the possibility of defeating these projectiles using explosively launched plates (Frey, Melani, and Stegall 1988; Hackbarth et al. 1992, 1993); however, because of difficulties associated with the use of explosives, alternative means of launching these metal plates are being considered. One method utilizes electromagnetic (EM) forces to generate the large accelerations needed for this purpose.

The "reconnection gun," developed by Cowan et al. (1987, 1991) is one example of an EM plate launcher. This is a multistage magnetic induction launcher, or coilgun, that has successfully launched a 150-g plate at a velocity of 1 km/s. The size and weight of a multistage device precludes its use on a vehicle; however, as a result, only single-stage devices have been considered in this program (Hummer and Hollandsworth 1991, 1992). One such design has been used to test the effectiveness of metal plates in defeating subscale metal rods (Hummer, Hollandsworth, and Berning 1995; Hummer 1996). Achieving launch velocities of several hundred meters per second with a single-stage device is a challenge as it requires internal stresses that peak at the several-hundred-ton level. This report contains descriptions of some of the modeling and simulation tools that have been developed to aid in the design of such launchers. These models have been particularly useful in identifying the key issues governing the performance of induction launchers. The efficacy of these tools is demonstrated by comparison with experiments.

2. Modeling EM Induction Plate Launchers

A magnetic induction launcher is a simple device that consists of an electromagnet coil (or coils) into which a conducting object (the projectile) is placed. The magnetic forces that launch the projectile evolve in the following manner: a constantly changing electric current is passed

through the magnet coil so that a changing magnetic field is produced in the bore of the launcher, the changing magnetic field will cause currents to flow in the conducting projectile, and the interaction between the magnetic field and these "induced" currents will result in a magnetic force being applied to the projectile, thus launching it out of the coil bore. Induction launchers are distinguished from other types of magnetic launchers, such as railguns, in that electrical currents are not directly applied to the projectile. The principle that current loops spontaneously form in the presence of a changing magnetic field is known as Faraday's Law of Induction (Halliday, Resnick, and Walker 1993). This is the same principle by which electrical transformers operate, and in fact the launcher can be thought of as the "primary" coil of a transformer, and the projectile itself is the "secondary" coil. It is useful to note that the induced currents will set themselves up in such a way as to cancel out magnetic fields within the volume of the conducting projectile. While the principle by which coilguns operate is simple, there are many launcher and projectile configurations to choose from, with no one being an obvious "optimal" choice for a particular application. The simulation tools described herein were developed specifically to identify the most effective design possible for a launcher of metal plates.

In order to predict launch coil effectiveness, a suite of computer programs has been developed that, when taken as a whole, serve to simulate the magnetic induction launch process. Brief descriptions of three such programs are:

- (1) The first simulates the acceleration of the plate and associated behavior of the launcher circuit, using key electrical parameters as a starting point (in particular the coil inductance as a function of plate position $L(x)$, which can be either measured directly or modeled via the following).
- (2) The second calculates the inductance of the coil with the plate either fully inserted ($L(0)$) or with the plate fully removed ($L(\infty)$), using the equation describing the inductance of a straight filament as a starting point. The quantity $\Delta L = L(\infty) - L(0)$ has proven to be a key indicator of performance.

- (3) The third uses simple magnetostatics to calculate the magnetic field around, and subsequently the magnetic forces on, the launch coil. This uses the equation for the magnetic field generated by a straight filament as a starting point.

When a simulacrum of a conducting plate (also based on filaments) is included, the forces on the plate can also be calculated. From these, the inductance gradient $dL(x)/dx$ can be inferred. This feature bypasses the need to perform any complex electrodynamic calculations.

These three programs can be used to assess and compare various hypothetical coil designs. The reasoning behind each of these models will be described in more detail in the following sections.

2.1 Plate Launch Mechanics. Only an overview of the system for modeling the acceleration of the plate will be presented because it has been described in detail in previous publications (Hummer and Hollandsworth 1991, 1992; Hummer 1996). The launcher's electrical circuit is essentially a series *RLC* circuit, as described in almost any introductory physics text (Halliday, Resnick, and Walker 1993). Applying Kirchhoff's Law for voltages in a loop to a series *RLC* circuit, the following differential equation can be obtained:

$$Q/C - IR - d(LI)/dt = 0, \quad (1)$$

where Q is the charge stored in the capacitor bank (used to power the launcher), C is the capacitance of the bank, I is the current in the circuit, R is the resistance of the circuit, L is the inductance of the circuit, and t is time. This system deviates from the simplest *RLC* circuit, in that L is not constant, but rather a function of plate position x , which itself is a function of time. There is also an additional equation describing the force on the plate during magnetic launch:

$$F = \frac{1}{2} I^2 \frac{dL}{dx}, \quad (2)$$

where dL/dx is the aforementioned inductance gradient function, which embraces all information regarding the magnetic coupling between coils and plate. For an existing coil, we assess the function $L(x)$ by simply connecting an inductance meter and making measurements while moving the plate in a stepwise fashion. For hypothetical coil designs, computer simulations can be used to approximate this function. In either case, a polynomial fit to the $L(x)$ data is used in the simulation code.

This picture of the launch process is of course highly simplified. In an actual system, the total circuit resistance will also depend on the plate position, as the plate itself is most definitely a part of the circuit. It in fact amounts to the secondary coil in a transformer circuit, which decouples from the primary coil (the launcher) as the plate is ejected. In addition, the use of large currents (hundreds of kA) will lead to joule heating, and the high-voltage switches used (e.g., spark gaps or ignitrons) are likely to behave somewhat nonlinearly. While more complex models do exist (Bernard 1987), the simple model described previously has proven to be quite sufficient for most purposes.

Figure 1 contains examples of dL/dx functions for two entirely different coil designs. The "box coil" design is a six-turn solenoid with a 5-in square cross section, with the plate inserted between the two center turns (similar to the one in Hummer [1996]). The "pancake coil" is comprised of two 6-in circular spirals (four turns each), one above and one below the plate. In both cases, a 4.5-in x 4.0-in x 0.25-in aluminum plate was used. Figure 1 exhibits both their respective $L(x)$ functions (as measured with an inductance meter) and the associated dL/dx functions. The overall change in inductance ($\Delta L = L(\infty) - L(0)$) was 0.62 μH for the box coil and 0.64 μH for the pancake coil.

The fact that the dL/dx functions peak at different locations leads to a slight difference in their respective coil's implementations. This arises from the fact that the force on the plate at any time is proportional to both I^2 and the value of dL/dx at the plate's current position. The current trace $I(t)$ resembles an underdamped sinusoid, and most of the acceleration occurs during the first

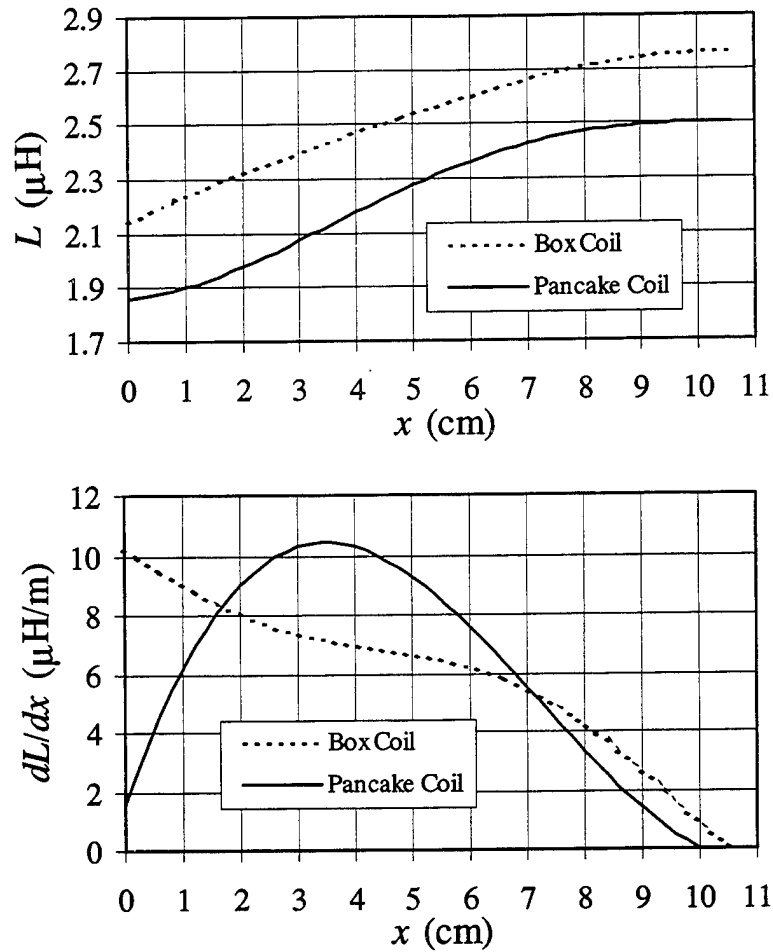


Figure 1. Inductance and Inductance Gradient vs. Plate Position for Two Different Coil Designs.

half-cycle. A higher final plate velocity (v_f) can therefore be achieved if one can arrange for the plate to be at or near the dL/dx peak position when $I(t)$ is reaching its first peak. This can be done through a careful choice of the plate's initial position (x_0). The fact that the box coil's dL/dx peak occurs at $x = 0$, however, precludes this possibility. As a result, the optimal x_0 value for the box coil is always $x_0 = 0$. In the pancake coil case, where dL/dx peaks at about $x = 4$ cm, the optimal x_0 value can range anywhere from 0.5 cm to 3.5 cm, depending on the launch parameters (plate mass m , initial bank voltage V_0 , etc.).

In order to model the launch of a plate, equations (1) and (2) are solved using a fourth-order Runge-Kutta technique (Burden and Faires 1985). As the launch generally occurs on a

millisecond time scale, a 1- μ s time step is often used. For an existing system, the actual capacitance (C), parasitic resistance (R), and parasitic inductance L_{sys} , where $L = L_{sys} + L(x)$, can either be approximated by fitting a measured $I(t)$ curve to a damped sinusoid (Hummer and Hollandsworth 1991, 1992; Hummer 1996) or determined more exactly by fitting to solutions for $I(t)$ generated by this model (see Figure 2). Both sets of parameters typically yield essentially equivalent predictions for the final plate velocity, which in turn tend to closely agree with measured values. This is illustrated in Table 1, where actual and predicted velocities are compared for three shots of the box coil.

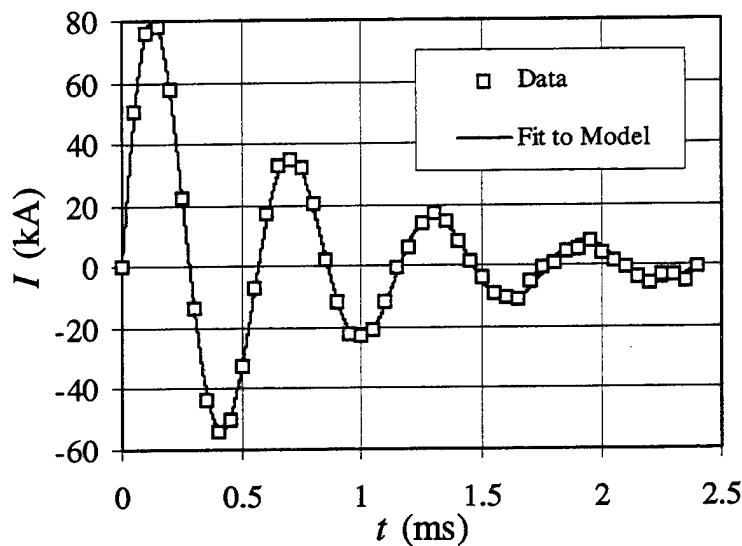


Figure 2. A Typical Fit of Plate Launch Model Results to Measured Current Data.

The plate launch model is useful for predicting and comparing the actual effectiveness of various coil designs. As a case in point, one might hypothesize that the pancake coil would be a better design than the box coil, because one can "tune" x_0 . Figure 3 shows that this is not the case, in that simulations predict almost identical v_f 's for both coils (for any given initial voltage V_0). The parameters used in these simulations were $C = 1,600 \mu\text{F}$, $L_{sys} = 2.0 \mu\text{H}$, $R = 15.0 \text{ m}\Omega$, and $m = 200 \text{ g}$. Predicted peak currents (a measure of peak stress on the coil) are also effectively

Table 1. A Comparison of Predicted vs. Actual Final Velocities for Three Shots of the Box Coil. Method No. 1 Uses R , L_{sys} , and C Values Derived from a Fit of $I(t)$ to a Damped Sinusoid. Method No. 2 Uses Values Derived from a Fit to Functions Generated by the Model Described in the Text.

Shot No.	V_0 (kV)	m (g)	Actual v_f (m/s)	v_f pred. (m/s) method no. 1	v_f pred. (m/s) method no. 2
15	14.00	208.14	185	184.5	186.7
16	13.99	206.87	186	185.2	186.5
17	13.99	217.33	176	177.8	179.2

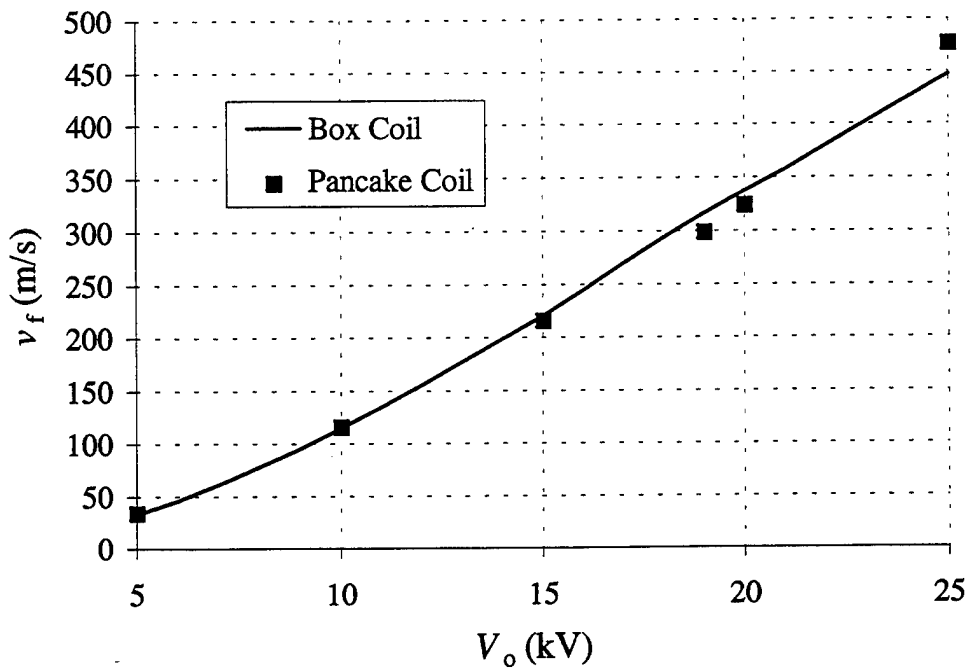


Figure 3. Theoretical Final Plate Velocities vs. Initial Voltage for Two Different Coil Designs.

identical. The nearly identical behavior of these coils is due to their nearly identical ΔL 's. The shapes of their $L(x)$ and dL/dx curves (Figure 1) seem to be relatively unimportant in determining their overall effectiveness.

The ability to simulate the launch process is essential if one wishes to compare the performance for different coil geometries and launch parameters. Table 2 contains the results of a comparison of four designs, including a hypothetical two-stage device based on round pancake coils. The triggering of the second stage was optimized in order to achieve the stated velocity and energy efficiency. Also included is a design based on squared spiral pancake coils, which proves to be twice as efficient as the round pancake coil case, even though a plate with twice the mass is used. The parameters used in each simulation were $V_0 = 20$ kV, $C = 1,600$ μ F, $L_{\text{sys}} = 1.5$ μ H, and $R = 15.0$ m Ω .

Table 2. A Comparison of Four Different Induction Launcher Designs Based on Simulations

Coil type	m (g)	V_f (m/s)	eff. (%)	I_{max} (kA)
box coil	200	350	3.8	331
round pancake	200	338	3.6	335
2 stage round pancake	200	432	5.8	333
square pancake	400	337	7.1	277

2.2 Inductance Calculations. As the parameter $\Delta L = L(\infty) - L(0)$ has proven to be a good indicator of overall launcher performance, it would be useful to be able to predict these values. The calculation of the inductance of the launcher coils without the plate present $L(\infty)$ is fairly straightforward. The coils are divided up into convenient segments, the self-inductance of each segment is calculated, and then the mutual inductance between each pair of segments is calculated. The total inductance of the coils is then simply the sum of all the self-inductances and mutual inductances. The situation when the plate is inside the coil $L(0)$ proves to be somewhat more complex because the mutual inductance between each segment and the entire plate must also be calculated. If the function dL/dx is available, it is much more convenient to calculate $L(0)$ using

$$L(0) = L(\infty) - \int_0^{\infty} (dL/dx) dx. \quad (3)$$

A simple method for calculating dL/dx is given in a later section.

2.2.1 Calculating Self-inductance With No Plate Present. Detailed descriptions of methods for calculating inductances can be found in Grover (1946) and., to a lesser extent, in Knoepfel (1970). As both books are now out of print, a synopsis will be provided here. The discussion will be restricted to coil structures that consist of a series of long, straight conductors that run either parallel or perpendicular to one another. These are sufficient to describe, or at least approximate, box coil and square pancake coil designs. The latter is similar to the round pancake coils described earlier, except that a squared spiral pattern is milled into the conductor plate.

Each segment of the coil structure is assumed to be a long, straight conductor of some length l , with arbitrarily shaped cross section having area A . For the purpose of calculating the segment's self-inductance, its cross section is divided into elemental areas ($dA = dx dy$), each representing a long, straight filament of the same length as the segment. The self-inductance of the segment is assumed to be the sum of the mutual inductances between all possible pairs of these parallel filaments. For a pair of parallel filaments, one located at (x, y) and the other at (x', y') , the exact mutual inductance is given by

$$dL_s = 0.002l \left[\ln \left(\frac{1}{d} + \sqrt{1 + \frac{l^2}{d^2}} \right) - \sqrt{1 + \frac{d^2}{l^2} + \frac{d}{l}} \right] dx dy dx' dy', \quad (4)$$

where l is the length of each segment, d is the distance between the segments, the distances are in centimeters, and the inductance is in microhenries. If the distance between the two filaments is much smaller than the length, this equation can be approximated by

$$dL_s = 0.002l \left[\ln \left(\frac{2l}{d} \right) - 1 \right] dx dy dx' dy'. \quad (5)$$

This can be integrated to find the total self-inductance of the segment

$$L_s = 0.002l \left[\ln(2l) - 1 \right] - \frac{1}{A^2} \int \int \int \int [\ln d] dx dy dx' dy'. \quad (6)$$

In keeping with convention, the last integral is related to a "geometric mean distance" ρ between all filaments covering the area A , which is defined by

$$\ln(\rho) = \frac{1}{A^2} \int \int \int \int [\ln d] dx dy dx' dy', \quad (7)$$

so that the self-inductance of the segment can be written as

$$L_s = 0.002l \left[\ln\left(\frac{2l}{\rho}\right) - 1 \right] \quad (8)$$

for any long conductor with any cross-sectional area, as long as the mean geometric distance across that area is known. The windings of box coils and square pancake coils have simple rectangular cross sections, and the integral in equation (8) can be expressed in closed form. The form of this equation is somewhat cumbersome, however, and it is far more convenient to use the approximation $\rho = 0.223(W + H)$, where W and H are the width and height of the rectangles, respectively. This equation was determined empirically; for example, one can calculate that $\rho = 0.22313(W)$ for a thin sheet ($H = 0$), and $\rho = 0.22353(2W)$ for a square ($H = W$). Using the approximate relation, it is a simple matter to calculate the total self-inductance of each segment. The total self-inductance of the coil is then simply the total of all of the segments' self-inductances.

2.2.2 Calculating Mutual Inductance With No Plate Present. One can express the mutual inductance between parallel segments of equal length in a similar fashion as before (once again assuming that distances are in centimeters and inductances are in microhenries);

$$L_M = \pm 0.002l \left[\ln\left(\frac{2l}{\rho_{ab}}\right) - 1 \right], \quad (9)$$

where l is the length of the segments, and, here, ρ_{ab} is the geometric mean distance between elements of the area of the first segment (A_a) and elements of the area of the second segment (A_b). Expressing the locations of arbitrary examples of these elements as (x_a, y_a) and (x_b, y_b) , ρ_{ab} is then defined by

$$\ln(\rho_{ab}) = \frac{1}{A_a A_b} \int \int \int \int [\ln d_{ab}] dx_a dy_a dx_b dy_b, \quad (10)$$

where d_{ab} is the distance between the area element in segment "a" and the area element in segment "b." The integral is analytic if both cross-sectional areas are rectangular; however, the final expression is once again rather complicated. In practice, ρ_{ab} is well approximated by the distance between the centers of the two rectangles, even when the segments are quite close together. Essentially, the total mutual inductance is calculated as if all of the coil segments were replaced by filaments located at their centers; the mutual inductances between all pairs of filaments are calculated and added together. The only difference between this and the self-inductance calculation is that the relative direction of current flow is now important: the term in equation (9) is positive if the currents are parallel, and negative if they are antiparallel. Pairs of segments in which the currents flow perpendicular to one another are of no concern, as it can be shown that their mutual inductances are zero.

As the segments in a square pancake coil are of unequal lengths, it behooves us to deal with this situation. Unequal-length filament cases can be broken down in a combination of several equal-length cases. For example, picture two parallel filaments with lengths l and m (where $l > m$) and separation d . Furthermore, assume that the longer filament extends past the shorter a distance p at one end and a distance q at the other (i.e., $l = m + p + q$). The mutual inductances between these filaments can then be calculated from four equal-length case terms;

$$2L_M = (L_{m+p} + L_{m+q}) - (L_p + L_q), \quad (11)$$

where the subscripts denote the filament length to be used in equation (9). The separation is d in all four cases. There are similar rules for cases in which the segments overlap differently or not at all (Grover 1946).

2.2.3 Results. Two aluminum pancake coil models were constructed in order to test this system, each consisted of two squared spiral coils with a center-to-center separation of 2 in. The first coil was constructed by milling out a 1/4-in wide square spiral pattern in a 6-in square plate of 1/4-in-thick aluminum, leaving behind 1/4-in square conductors. There were five turns in each coil. The second was constructed similarly, except that 1/2-in conductors and spaces were formed for a total of two and a half turns in each coil. In both cases, all inside corners in the conductors were left with a round fillet with a radius equal to that of the milling bit used (a feature not included in the calculations). Several of the conductor segments are not long compared to their widths, in which case the validity of equation (8) comes into question. Even so, the agreement was excellent: the total inductance of the five-turn coils was calculated to be 5.92 μH and measured to be 5.91 μH . In the two-and-a-half-turn case it was 1.48 μH (calculated) vs. 1.54 μH (measured).

2.2.4 Calculating Inductances With a Plate Present. The scheme for estimating the inductance of these coils with a metal plate inserted is somewhat cumbersome, and only a brief description will be provided. The difficulty is in modeling the plate itself, as it is a conductor whose length and width are comparable and in which eddy currents flow in a complex pattern. The scheme relies on Lenz's Law (Halliday, Resnick, and Walker 1993), which implies that the eddy currents will form in such a way as to largely cancel the field within the volume of the plate. Another way of looking at this is that the plate tends to shield the top coil from the bottom (it would isolate them completely if the plate covered an area much larger than the coils themselves). So, even though the plates actually only cover the same area as the coils (and thus some leakage around the edges is likely), it is assumed that there is no mutual inductance between any of the upper and lower coil segments, and these terms are simply excluded from the previous calculation.

Each of the two coils does have mutual inductance with the plate, however, and this must be accounted for. In order to mimic the cancellation of field at the plate surface, an "image coil" is constructed on the opposite side of the launcher's midplane. This image coil is identical to the real coil in all ways, except that the current flows through it in the opposite direction, and, thus,

symmetry guarantees that the fields will cancel at their midplane. The mutual inductance of the coil/plate combination is then assumed to be the same as that for the coil/image coil combination. An identical procedure is then applied to the other coil, and all terms are added.

The results for this calculation are not quite as good as in the previous case: the inductance calculated for the five-turn coils was 3.51 μH , as compared to a measured value of 3.58 μH . For the two-and-a-half-turn case it was 0.85 μH (calculated) vs. 1.01 μH (measured). Possible sources of error include imperfect isolation of the upper and lower coils and the fact that the plate's self-inductance is not accounted for. This model has proven to be of limited usefulness because it cannot easily be extended to cases where the plate offers only partial shielding. The following model offers a way to gain this information, while also yielding estimates of the intracoil stresses and external magnetic fields and, so, will be described in more detail.

2.3 Quasi-static Model. The launch of a plate by magnetic induction is a highly dynamic process: the current in the coil is changing in time; the magnetic field and eddy currents induced in the plate change along with it; the magnetic field attempts to diffuse into the edges of all conductors; the temperature and, thus, resistivity of the conductors rise, etc. Most of these events can be simulated by the application of Maxwell's equations, which govern all classical EM behavior. In practice, however, it is extremely difficult to apply the equations to arbitrary three-dimensional situations. This was the motivation behind the conception of the following model, first described in (Berning et al. 1997), which conveniently ignores much of the three-dimensional nature of the problem and almost all of its dynamic nature.

2.3.1 Magnetic Field and Lorentz Force Calculations. The primary function this model is to estimate the magnetic field \vec{B} created by the coil assembly. Considering the case where no plate is present, we begin by assuming that the magnitude of the field (at any point) at a particular time is proportional to the current in the coil at that time. As such, we completely ignore delayed responses of the system. It also implies that no ferromagnetic material is present in the vicinity. This assumption allows us to calculate the field using magnetostatics. Furthermore, we exploit the fact that the B -field outside of a length of conductor of finite cross section tends to resemble

the field due to an infinitesimally thin filament of the same length, which is simple to describe. For a finite length filament carrying current I and oriented parallel to the x -axis, having endpoint coordinates (x_{01}, y_0, z_0) and (x_{02}, y_0, z_0) , the magnetic field components at an arbitrary point in space (x, y, z) are, in MKS units,

$$B_x = 0,$$

$$B_y = - \left(\frac{I\mu_0}{4\pi} \right) (z - z_0) \left[\frac{1}{(x_{02} - x)r_2 - (r_2)^2} - \frac{1}{(x_{01} - x)r_1 - (r_1)^2} \right],$$

and

$$B_z = + \left(\frac{I\mu_0}{4\pi} \right) (y - y_0) \left[\frac{1}{(x_{02} - x)r_2 - (r_2)^2} - \frac{1}{(x_{01} - x)r_1 - (r_1)^2} \right],$$

where

$$r_1 = \sqrt{(x - x_{01})^2 + (y - y_0)^2 + (z - z_0)^2},$$

and

$$r_2 = \sqrt{(x - x_{02})^2 + (y - y_0)^2 + (z - z_0)^2}. \quad (12)$$

Alternate orientations would require the appropriate coordinate transformation. One practical concern involving the equation (12) is that it yields " ∞ " at all points along the segment itself. This is due to the unphysical assumption of zero thickness and can be alleviated in a simulation program by forcing B to zero within some arbitrarily tiny distance around the segment itself.

The program "BFIELD10" has the ability to simulate coil structures with combinations of filamentary segments, provided each is oriented in either the x , y , or z directions. Currently, it can automatically construct pancake coils consisting of concentric rectangles or rectangular

spirals, given the required dimensions. It can also approximate the structure of a box coil with coaxial rectangular loops. It then calculates magnetic field strength and direction and can display these graphically. It also estimates the magnetic forces felt by various sections of the launcher by dividing each filament into a number of segments and then calculating the Lorentz force F felt by that segment. The Lorentz force is given by (Halliday, Resnick, and Walker 1993):

$$\vec{F} = I \vec{L} \times \vec{B} , \quad (13)$$

where L is the length of the segment, and B is the field at the segment's center. These results can also be displayed graphically.

2.3.2 Plate Models and Inductance Gradient Calculations. The aforementioned system treats the coil assembly as if it were a simple DC electromagnet. This makes it difficult to model the plate because all of the currents present in the plate during launch are a direct result of the changes in the magnetic field. Lenz's Law implies that the eddy currents induced in the plate will take forms that attempt to cancel the field within the plate itself and will constantly adjust to follow the external field. How well these currents succeed in expelling the field depends on the conductivity of the plate; a perfect conductor would have zero field throughout its volume, and a less than perfect conductor would allow some field in along its outer surfaces. The characteristic distance of penetration is referred to as the "skin depth," and is typically less than 2 mm for the metals and frequencies used in this study (Knoepfel 1970). The actual eddy currents that perform this feat clearly must possess a highly detailed, three-dimensional structure, and determining that structure would require a difficult three-dimensional electrodynamic calculation.

The following model, which uses a finite number of filaments to model the plate, must therefore forego any attempt at an exact simulation. Furthermore, the complex electrodynamic process is in no way simulated, but rather, the effect is. The scheme is as follows: (1) a coil design and current are chosen, and its magnetic field is simulated previously mentioned; (2) a basic structure of filamentary loops is developed in order to simulate the plate; then (3) the currents within these "plate" filaments are adjusted in such a way as to minimize (not cancel) the

magnetic field within the plate. This last step is simply an attempt to mimic the expulsion of magnetic field from the plate. The coarseness of a filamentary loop structure precludes an exact cancellation, so we are forced to resort to some sort of minimization scheme.

The question now becomes: what is the simplest combination of plate structure and minimization scheme that will yield an adequate approximation of the situation? The method for determining "adequacy" is quite simple; once the currents in them are set, the magnetic forces on the plate filaments can be calculated in the same fashion as for the coil filaments and then added in order to find the net magnetic force on the plate. If the expulsion of the field has been adequately approximated, then the value of dL/dx can be inferred using equation (2), even though no proper inductance calculation has been performed. Functions derived in this manner are then compared to measured functions in order to evaluate the particular scheme used.

In order to illustrate the level of complexity required by this model, a brief history of its evolution follows. The first version used a single rectangular loop covering the same area as the plate, with its current adjusted so that the field at the plate's central point is zero. When tested on the square pancake design mentioned previously, this yielded dL/dx curves that were poorly shaped and far too high. Recognizing the fact that the coil's field tends to have different directions inside and outside the coil the next plate model broke the plate into two loops: one covering the area of the plate inside the coil and one covering the area of the plate outside, so that these regions would be handled separately. When the two plate-loop currents were adjusted to cancel the field at their respective loops' central points, the resulting dL/dx curves took on an excellent shape, but were still at least a factor of 3 too high. At this point, a new minimization scheme was tried: forcing the average of the field's vertical components inside a particular loop to go to zero. A finite number of points within the loop were used in order to determine the average, and, at first, 25 equally spaced points were used. This immediately yielded a near perfect dL/dx curve for the square pancake model, with the same excellent shape and normalization about 10% off. Splitting each loop into an "upper" and "lower" one, in order to mimic the three-dimensional nature of the plate, improved the agreement even further.

Unfortunately, this remarkable agreement proved to be partially the result of a fortuitous choice of sampled points, as the normalization of the inferred dL/dx curve was later shown to be highly sensitive to the number and spacing of said points. In fact, the spacing of the 25 points can arbitrarily be adjusted so that the inferred curve is a near perfect fit to the data, at least in this one case. Using larger numbers of points tended to degrade the fit. The presence of arbitrary parameters (i.e., the number and spacing of sampled points) led to the abandonment of this scheme. It is instructive, however, to note just how little filamentary structure is needed in order to obtain reasonable semiquantitative results.

While the four-loop model gave reasonable results using the minimization of average field scheme, it clearly lacked sufficient structure to mimic the actual cancellation of the complex coil field. For this reason, more structure was added in the final version of the model: the plane of the plate is divided into 100 equally sized rectangular areas, and two rectangular loops (an upper and lower) are used in each region, as illustrated in Figure 4. The current in each loop pair is adjusted so that the vertical component of the B field at the central point of their volume is zero. In practice, the plate currents are adjusted so that their fields are opposite what is produced by the coil. As the plate's field now has contributions from each of the 100 plate loop pairs, adjusting the 100 plate loop currents to simultaneously zero, the field at the 100 points becomes somewhat complicated. However, since each loop's contribution is proportional to that loop's current, and the total is just the sum of these contributions, the problem lends itself to linear algebra. As this problem requires the reduction of a 100 x 100 matrix, a highly efficient numerical method (such as "LU decomposition" [Press et. al 1986]) is recommended. This feature is included in the program BFIELD10.

Figure 5 illustrates the effectiveness of the 200-loop model; it compares BFIELD10 results with measured results for the 6-in x 6-in square pancake described previously. The coil-center to coil-center spacing was 2 in, and the plate was a 6-in x 6-in x 0.25-in piece of aluminum. The dL/dx results for a crude replica of the coil, made from thin copper wire, are also shown. The close resemblance of the replica's dL/dx curve to that for the actual coil is typical, a fact that

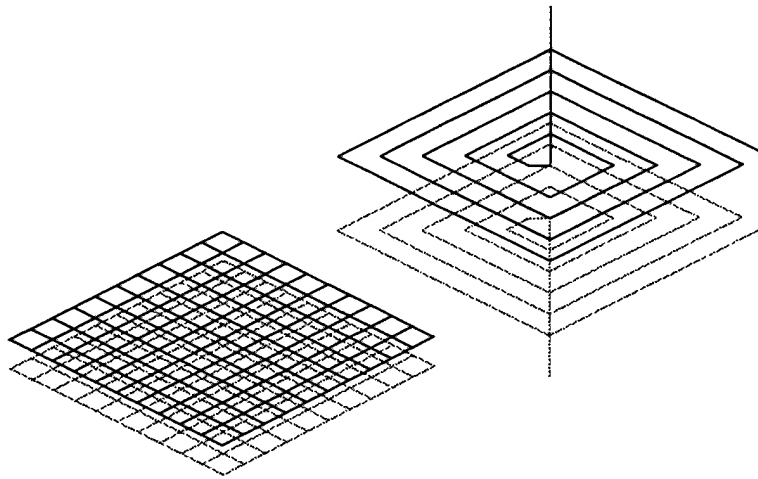


Figure 4. Filamentary Structures Used to Model a Square Plate and Square Pancake Coil System.

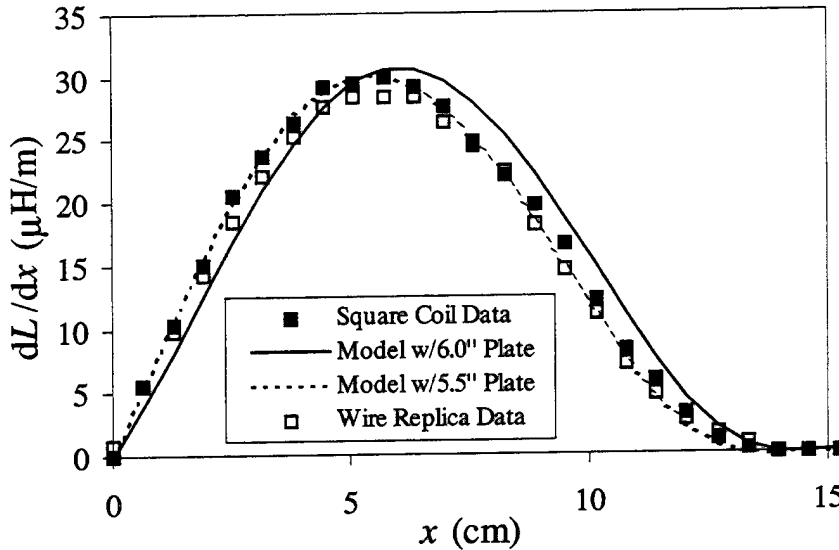


Figure 5. Measured Inductance Gradient of a 6-in Square Pancake Coil Compared to the Results of Simulations Performed by the Program BFIELD10 (for Both the Actual 6-in Square Plate and a Hypothetical 5.5-in Square Plate). Also Included Are Data from a Narrow Gauge Wire Replica of the Coil.

makes replicas a useful, inexpensive method of testing different coil designs (although their $L(x)$ curves differ by a constant, due to the thin wire's large self-inductance). As seen Figure 5, the simulated dL/dx curve is slightly higher than and offset from the measured curves. This offset was not seen in the previous four-loop model and is suspected to be an artifact associated with this particular plate model. Simulations using lesser numbers of plate loops (50, 72, 98, 128, and

162) show a reasonable convergence toward the 200-loop answer and indicate that more loops would not improve the agreement significantly.

Experience indicated that both the normalization and the offset could be improved if one assumed an "effective" plate size smaller than the actual size. Figure 5 includes results of simulations in which a 5.5-in x 5.5-in plate size was assumed, and these are indeed a better fit to the measured results. This improvement is also seen in Figure 6, where simulated and actual results for a 10-in x 6-in square pancake coil and 12-in x 6-in plate are found, assuming an 11.5-in x 5.5-in plate once again improved the fit. It would be tempting to explain the efficacy of "discounting" the plate's edges by invoking some sort of skin-depth argument; however, the 0.25-in adjustments to each edge are much larger than the <0.08-in skin depth expected here, It may be an indication that the situation near the edges is not being properly treated, however, and perhaps a finer mesh there would improve the fit. Regardless, the unadulterated 200-loop model, for all its crudity, is still a remarkably effective device.

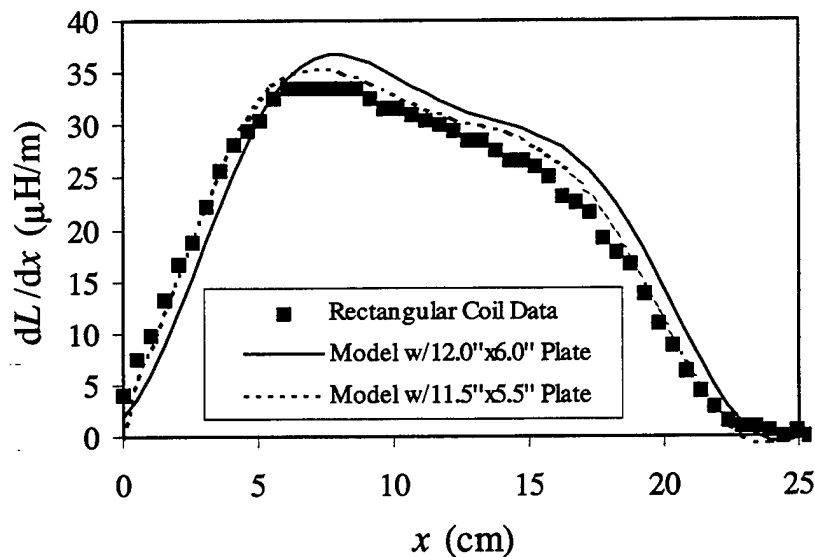


Figure 6. Measured Inductance Gradient of a 10-in x 6-in Rectangular Pancake Coil Model Compared to the Results of Simulations (for Both the Actual 12-in x 6-in Plate and an 11.5-in x 5.5-in Plate).

2.3.3 Magnetic Field Results. The magnetic fields generated by this type of plate launcher have been the objects of two prior studies; one concerning a round pancake coil (Coburn, Le, and Martin 1995) and the other dealing with a square pancake coil design (Berning et al. 1997). As the quasi-static model was utilized in the latter study, a brief discussion of the outcome will be included here.

The launcher in question consisted of two 6-in-wide, 4 1/2-turn square pancake coils, machined from a copper-beryllium alloy. The conductors were 0.25 in wide and 0.5 in high, with 0.25 in of space between them. The coils were completely encased in a glass-epoxy composite (G10) support structure, and 14-in-long sections of steel U-channel were added to the top and bottom in order to stiffen the structure. The aluminum alloy plates were 6 in square \times 0.25 in thick and had a mass of 400 g. The launcher was fired many times from a small test stand, depicted in Figure 7, which contained a 100-kJ capacitor bank.

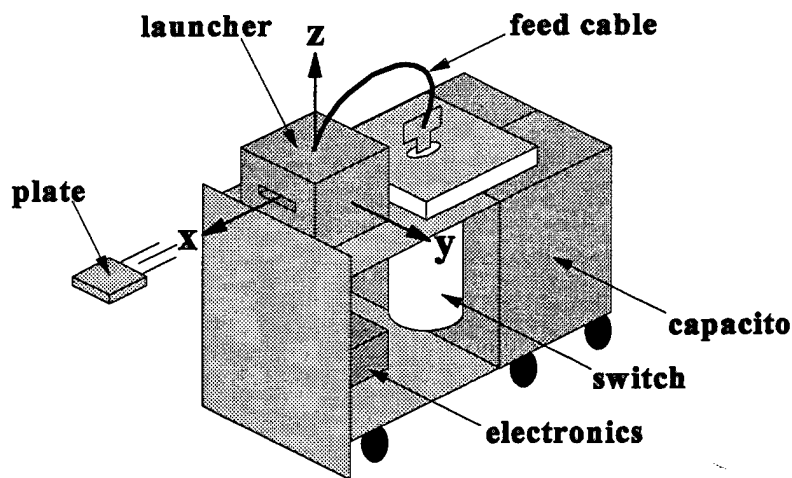


Figure 7. The Test Stand Used in a Study of the EM Fields Generated by an Induction Launcher.

The three components of magnetic field were measured at 10 separate points, some along the shotline, some beside the launcher. As expected, the time evolution of the magnetic field followed that of the launcher current. Figure 8 contains a plot of peak field strength vs. radial distance from the center of the launcher for all points. The complex structure seen in Figure 8 would seem to belie the simple power-law response predicted by the quasi-static model (depicted by the solid line); however, inclusion of the power-feed cable in the model recreates most of the structure. The power-feed cable was clearly the dominant source of field in some locations.

The level of agreement between simulation and reality seen in Figure 8 would appear to be quite reasonable, especially since the simulations do not include the effects of shielding by the various metallic structures in and around the launcher (except by the plate), nor are all current paths included.

2.3.4. Intracoil Stresses. The quasi-static model can also estimate the forces on sections of the coil itself, as illustrated in Figure 9, in which forces acting on select parts of a square pancake coil are illustrated. Forces are highest in the region behind the plate, as the field is concentrated by the exclusion effect. Forces are also concentrated at corners, with total magnitudes on the order of 140 ksi at the 300-kA level. This is near the 155-ksi yield-strength limit for the copper-beryllium alloy used to construct a launcher much like the one depicted. Based on this simulation, one might therefore conclude that this launcher could survive a 300-kA pulse; however, the situation is much more complex than this. In fact, this launcher failed (via cracks at two rear corners) at a peak current level of approximately 200 kA, at which point the internal stresses are less than half that seen for 300 kA.

This apparent underestimation of internal stresses should not be entirely unexpected, as the assumption of filamentary conductors is certain to result in poor estimations of the field strength in regions close to the filaments themselves. In particular, the effect of shielding by the conductor sections is completely omitted. The "pinching" of the field lines caused by the exclusion of field from the conductor sections may well increase the field between adjacent lengths of conductor by nearly a factor of 2 in this design, as the gaps through which the field

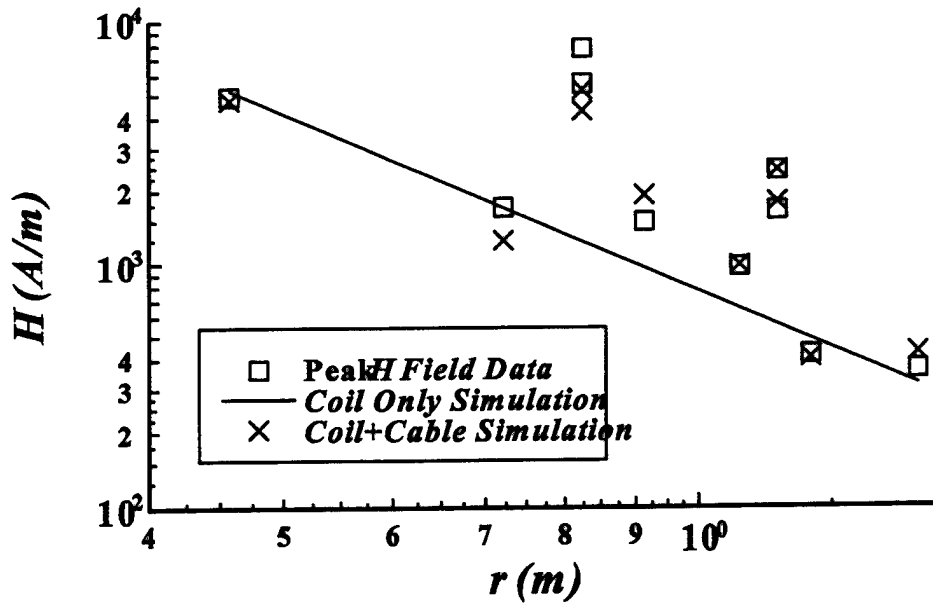


Figure 8. The Magnitude of the Measured Magnetic Field Compared to Simulations. Note That the Complex Pattern Is Largely Due to the Presence of the Feed Cable.

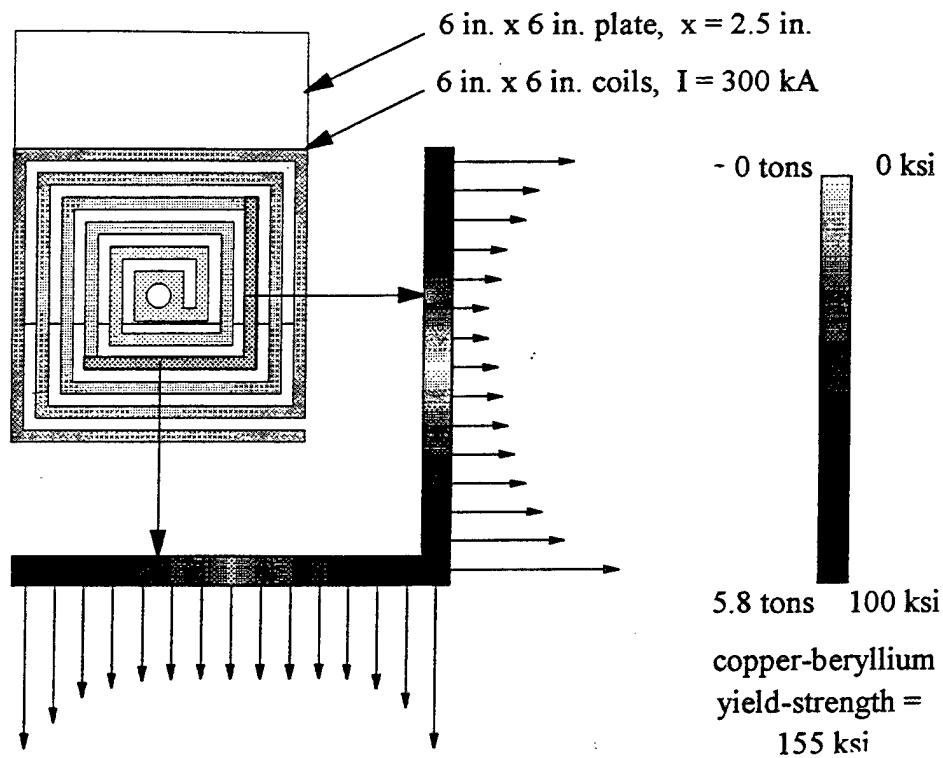


Figure 9. Calculated Forces on One Section of a Square Pancake Coil.

must thread only cover 50% of the coil's area. Since the exact extent of this effect is not calculated, internal stress estimations can only be described as semi-quantitative. However, this information is still quite useful for engineering purposes.

3. Conclusion

The three models described here have proved vital in the development of an understanding of the key issues in induction launcher design. Based on the results of modeling, certain rules of thumb have been developed:

- (1) For the best coil/plate coupling, the plate's area should be equal to or greater than the area of the magnet's bore. This guarantees that most of the field lines will be forced to bend behind the plate, where they do the most good. Plates smaller than the bore will have field lines bending around their sides, so that there are forces "squeezing" the two sides of the plate together. As these forces are at right angles to the direction of travel and tend to cancel in any event, they represent wasted effort. The use of small plates explains, in large part, the poor efficiency of the box coil and round pancake coil designs. The square pancake coil design uses plates with the same area as the coils. One price to be paid for this improvement is a somewhat weaker structure, as the slot that holds the plate offers less support against forces attempting to squeeze it shut.
- (2) Coil conductor sections closer to the plate yield the highest fields and forces, so it is best to have as many near the plate as possible. This suggests that a pancake coil design, where all sections are equally close to the plate, might be superior. A serpentine coil also offers this level of proximity, but generates relatively small fields.

This latter comment raises some questions concerning the relative performance of the box coil, round pancake coil, and square pancake coil designs used in these studies. The nearly identical performance of the box coil and round pancake coil can be explained by the fact that the box coil had a conductor section running directly behind (and actually in contact with) the plate. The proximity to the rear of the plate, along which the largest eddy currents flow, explains why the box coil performed so well; sections further from the plate added much less to the performance. In addition, the pinching effect on the field between this section of conductor and the plate may amplify the launch forces. In the pancake coil designs described here, there were no equivalent conductor sections, as the bus bars connecting the upper and lower coils ran vertically down one corner. The latest pancake coil designs now have a bus bar that runs down one corner behind (and in contact with) the plate and then down to the bottom coil. This is expected to improve performance considerably.

The explanation for why the square pancake coil design outperforms (in terms of measured ΔL) the round pancake coil design (even when bore-sized plates were used) may be more subtle. One explanation is based on the idea that two linear, antiparallel currents elements repel one another more effectively than curved elements would because the Lorentz forces along their lengths are all in the same direction. In the case of curved elements, some components of the Lorentz forces would tend to cancel each other out, wasting effort. Thus, it may be the fact that the square pancake coil offers more linear segments that are parallel to the major eddy current element running along the back of the plate that explains the improved coil/plate coupling.

In any event, the square pancake coil design would seem to epitomize these ideas concerning performance improvement. It also carries the added benefit of being naturally compact, so that more launchers can be mounted on a vehicle. One disadvantage that always accompanies increased performance, however, is increased intracoil stresses. Future design efforts will center about containing these stresses more effectively.

4. References

- Bernard, M. J. "Electromagnetic Acceleration of a Metallic Carrier Plate: Experiment and Computer Simulation." Master's Thesis, The State University of New York at Buffalo, 1987.
- Berning, P. R., C. R. Hummer, C. D. Le, and W. O., Coburn. "A Theoretical and Experimental Study of the Electromagnetic Environment Surrounding a Magnetic Induction Launcher." *IEEE Transactions on Magnetics*, vol. 33, no. 1, pp. 368-372, January 1997.
- Burden, R. L., and J. D. Faires. *Numerical Analysis*. Boston: Prindle, Weber, and Schmidt Publishers, 3rd ed., 1985.
- Coburn, W., C. Le, and H. Martin. "Electromagnetic Field Measurements Near a Single Stage Reconnection Gun." ARL-MR-206, U.S. Army Research Laboratory, Aberdeen Proving Ground, MD, April 1995.
- Cowan, M. PA-APPL-7-034 354, Sandia National Laboratories, 6 April 1987.
- Cowan, M., M. Widner, E. C. Cnare, B. W. Duggin, R. J. Kaye, and J. R. Freeman. Exploratory Development of the Reconnection Launcher 1986-1990." *Proc. IEEE Trans. Magnetics*, vol. 27, no. 1, pp. 563-567, Sandia National Laboratories, January 1991.
- Frey, R. B., G. Melani, and S. R. Stegall. "Interaction Between Kinetic Energy Penetrators and Reactive Armor." BRL-TR-2964, U.S. Army Ballistic Research Laboratory, Aberdeen Proving Ground, MD, October 1988.
- Grover, F. W. "Inductance Calculations Working Formulas and Tables," New York: Dover Publications, 1946.
- Hackbarth, D., G. Bulmash, M. Zoltowski, M. Wilkins, and A. Kusubou. "Momentum Transfer Armor." *Proceedings of the 1992 Combat Vehicle Survivability Symposium*, Gaithersburg, MD, April 1992.
- Hackbarth, D., M. Zoltowski, M. Wilkins, and A. Kusubou. "Momentum Transfer Armor." *Proceedings of the 1993 Combat Vehicle Survivability Symposium*, Gaithersburg, MD, April 1993.
- Halliday, D., R. Resnick, and J. Walker. *Fundamentals of Physics, Extended*. 4th ed., John Wiley and Sons, Inc., New York, 1993.

- Hummer, C. R., C. E. Hollandsworth. "Launching of Flat Plates with a Single-Stage Reconnection Gun." *Proceedings of the Eighth International Pulse Power Conference*, IEEE cat. no. CH3052-8, San Diego, CA, June 1991.
- Hummer, C. R., C. E. Hollandsworth. "A Single-Stage Reconnection Gun." ARL-TR- 14, U.S. Army Research Laboratory, Aberdeen Proving Ground, MD, November 1992.
- Hummer, C. R., C. E. Hollandsworth, and P. R. Berning. "Interactions Between Subscale Rods and Electromagnetically Launched Metal Plates." *Proceedings of the 3rd International Symposium on Classified and Controlled Topics*, November 1995.
- Hummer, C. R. "Test of an Electromagnetic (EM) Launcher for Flat Plates." ARL-TR- 105 3, U.S. Army Research Laboratory, Aberdeen Proving Ground, MD, April 1996.
- Knoepfel, H. *Pulsed High Magnetic Fields*. Amsterdam: North-Holland Publishing Company, 1970.
- Press, W. H., B. P. Flannery, S. A. Teukolsky, and W. T. Vetterling, *Numerical Recipes*, Cambridge University Press, Cambridge, 1986.

<u>NO. OF COPIES</u>	<u>ORGANIZATION</u>
2	DEFENSE TECHNICAL INFORMATION CENTER DTIC DDA 8725 JOHN J KINGMAN RD STE 0944 FT BELVOIR VA 22060-6218
1	HQDA DAMO FDQ DENNIS SCHMIDT 400 ARMY PENTAGON WASHINGTON DC 20310-0460
1	CECOM SP & TRRSTRL COMMCTN DIV AMSEL RD ST MC M H SOICHER FT MONMOUTH NJ 07703-5203
1	PRIN DPTY FOR TCHNLGY HQ US ARMY MATCOM AMCDCG T M FISETTE 5001 EISENHOWER AVE ALEXANDRIA VA 22333-0001
1	PRIN DPTY FOR ACQUSTN HQS US ARMY MATCOM AMCDCG A D ADAMS 5001 EISENHOWER AVE ALEXANDRIA VA 22333-0001
1	DPTY CG FOR RDE HQS US ARMY MATCOM AMCRD BG BEAUCHAMP 5001 EISENHOWER AVE ALEXANDRIA VA 22333-0001
1	ASST DPTY CG FOR RDE HQS US ARMY MATCOM AMCRD COL S MANESS 5001 EISENHOWER AVE ALEXANDRIA VA 22333-0001

<u>NO. OF COPIES</u>	<u>ORGANIZATION</u>
1	DPTY ASSIST SCY FOR R&T SARD TT F MILTON THE PENTAGON RM 3E479 WASHINGTON DC 20310-0103
1	DPTY ASSIST SCY FOR R&T SARD TT D CHAIT THE PENTAGON WASHINGTON DC 20310-0103
1	DPTY ASSIST SCY FOR R&T SARD TT K KOMINOS THE PENTAGON WASHINGTON DC 20310-0103
1	DPTY ASSIST SCY FOR R&T SARD TT B REISMAN THE PENTAGON WASHINGTON DC 20310-0103
1	DPTY ASSIST SCY FOR R&T SARD TT T KILLION THE PENTAGON WASHINGTON DC 20310-0103
1	OSD OUSD(A&T)/ODDDR&E(R) J LUPO THE PENTAGON WASHINGTON DC 20301-7100
1	INST FOR ADVNCD TCHNLGY THE UNIV OF TEXAS AT AUSTIN PO BOX 202797 AUSTIN TX 78720-2797
1	DUSD SPACE 1E765 J G MCNEFF 3900 DEFENSE PENTAGON WASHINGTON DC 20301-3900
1	USAASA MOAS AI W PARRON 9325 GUNSTON RD STE N319 FT BELVOIR VA 22060-5582

<u>NO. OF COPIES</u>	<u>ORGANIZATION</u>
1	CECOM PM GPS COL S YOUNG FT MONMOUTH NJ 07703
1	GPS JOINT PROG OFC DIR COL J CLAY 2435 VELA WAY STE 1613 LOS ANGELES AFB CA 90245-5500
1	ELECTRONIC SYS DIV DIR CECOM RDEC J NIEMELA FT MONMOUTH NJ 07703
3	DARPA L STOTTS J PENNELLA B KASPAR 3701 N FAIRFAX DR ARLINGTON VA 22203-1714
1	SPCL ASST TO WING CMNDR 50SW/CCX CAPT P H BERNSTEIN 300 O'MALLEY AVE STE 20 FALCON AFB CO 80912-3020
1	USAF SMC/CED DMA/JPO M ISON 2435 VELA WAY STE 1613 LOS ANGELES AFB CA 90245-5500
1	US MILITARY ACADEMY MATH SCI CTR OF EXCELLENCE DEPT OF MATHEMATICAL SCI MDN A MAJ DON ENGEN THAYER HALL WEST POINT NY 10996-1786
1	DIRECTOR US ARMY RESEARCH LAB AMSRL CS AL TP 2800 POWDER MILL RD ADELPHI MD 20783-1145

<u>NO. OF COPIES</u>	<u>ORGANIZATION</u>
1	DIRECTOR US ARMY RESEARCH LAB AMSRL CS AL TA 2800 POWDER MILL RD ADELPHI MD 20783-1145
3	DIRECTOR US ARMY RESEARCH LAB AMSRL CI LL 2800 POWDER MILL RD ADELPHI MD 20783-1145
<u>ABERDEEN PROVING GROUND</u>	
2	DIR USARL AMSRL CI LP (305)

NO. OF
COPIES ORGANIZATION

ABERDEEN PROVING GROUND

27 DIR USARL
AMSRL WM
DR D ECCLESHALL
AMSRL WM W
DR C H MURPHY
AMSRL WM WM
DR P BERNING
DR R BOSSOLI
AMSRL WM WD
DR S CORNELISON
J CORRERI
D DANIEL
DR A GAUSS
DR C HOLLANDSWORTH
DR C HUMMER
DR L KECSKES
DR T KOTTKE
K MAHAN
DR M MCNEIR
F PIERCE
DR J POWELL
DR A PRAKASH
S ROGERS
C STUMPFEL
DR G THOMSON
AMSRL WM WG
DR L PUCKETT
AMSRL WM P
DR P KASTE
AMSRL WM PA
G KATULKA
AMSRL WM PB
A ZIELINSKI

INTENTIONALLY LEFT BLANK.

REPORT DOCUMENTATION PAGE			Form Approved OMB No. 0704-0188	
Public reporting burden for this collection of information is estimated to average 1 hour per response, including the time for reviewing instructions, searching existing data sources, gathering and maintaining the data needed, and completing and reviewing the collection of information. Send comments regarding this burden estimate or any other aspect of this collection of information, including suggestions for reducing this burden, to Washington Headquarters Services, Directorate for Information Operations and Reports, 1215 Jefferson Davis Highway, Suite 1204, Arlington, VA 22202-4302, and to the Office of Management and Budget, Paperwork Reduction Project (0704-0188), Washington, DC 20503.				
1. AGENCY USE ONLY (Leave blank)	2. REPORT DATE June 1997	3. REPORT TYPE AND DATES COVERED Final, Jun 94 - Aug 96		
4. TITLE AND SUBTITLE Magnetic Induction Launcher Models			5. FUNDING NUMBERS PR: 1L162618AH80	
6. AUTHOR(S) Paul R. Berning and Charles R. Hummer				
7. PERFORMING ORGANIZATION NAME(S) AND ADDRESS(ES) U.S. Army Research Laboratory ATTN: AMSRL-WM-WD Aberdeen Proving Ground, MD 21005-5066			8. PERFORMING ORGANIZATION REPORT NUMBER ARL-TR-1384	
9. SPONSORING/MONITORING AGENCY NAMES(S) AND ADDRESS(ES)			10. SPONSORING/MONITORING AGENCY REPORT NUMBER	
11. SUPPLEMENTARY NOTES				
12a. DISTRIBUTION/AVAILABILITY STATEMENT Approved for public release; distribution is unlimited.			12b. DISTRIBUTION CODE	
13. ABSTRACT (Maximum 200 words) Various computer models developed to aid in the design of magnetic induction launchers or coilguns are described. The first models the launch process based on launcher circuit parameters, in particular, the coil inductance as a function of projectile position $L(x)$. The second set of models calculates the overall inductance of the launcher coil both with and without the plate present. The difference between the values $\Delta L = L(\infty) - L(0)$ has proven to be a key parameter in determining the relative performance of different launcher designs. The third set of models estimate the fields and forces generated by the launcher, under the assumption of filamentary conductor structures and static conditions. The methods used to avoid the complications associated with the dynamic nature of the actual launch process are described. These last models yield an inductance gradient function dL/dx that is crucial for the assessment of launcher performance. The usefulness of these models has been demonstrated in a project to design a coilgun that launches metal plates against incoming kinetic energy (KE) penetrators.				
14. SUBJECT TERMS electromagnetic launch, active protection			15. NUMBER OF PAGES 35	
			16. PRICE CODE	
17. SECURITY CLASSIFICATION OF REPORT UNCLASSIFIED	18. SECURITY CLASSIFICATION OF THIS PAGE UNCLASSIFIED	19. SECURITY CLASSIFICATION OF ABSTRACT UNCLASSIFIED	20. LIMITATION OF ABSTRACT UL	

INTENTIONALLY LEFT BLANK.

USER EVALUATION SHEET/CHANGE OF ADDRESS

This Laboratory undertakes a continuing effort to improve the quality of the reports it publishes. Your comments/answers to the items/questions below will aid us in our efforts.

1. ARL Report Number/Author ARL-TR-1384 (Berning) Date of Report June 1997

2. Date Report Received _____

3. Does this report satisfy a need? (Comment on purpose, related project, or other area of interest for which the report will be used.) _____

4. Specifically, how is the report being used? (Information source, design data, procedure, source of ideas, etc.) _____

5. Has the information in this report led to any quantitative savings as far as man-hours or dollars saved, operating costs avoided, or efficiencies achieved, etc? If so, please elaborate. _____

6. General Comments. What do you think should be changed to improve future reports? (Indicate changes to organization, technical content, format, etc.) _____

CURRENT
ADDRESS

Organization

Name

E-mail Name

Street or P.O. Box No.

City, State, Zip Code

7. If indicating a Change of Address or Address Correction, please provide the Current or Correct address above and the Old or Incorrect address below.

OLD
ADDRESS

Organization

Name

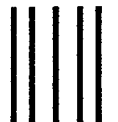
Street or P.O. Box No.

City, State, Zip Code

(Remove this sheet, fold as indicated, tape closed, and mail.)
(DO NOT STAPLE)

DEPARTMENT OF THE ARMY

OFFICIAL BUSINESS



NO POSTAGE
NECESSARY
IF MAILED
IN THE
UNITED STATES

BUSINESS REPLY MAIL
FIRST CLASS PERMIT NO 0001,APG,MD

POSTAGE WILL BE PAID BY ADDRESSEE

DIRECTOR
US ARMY RESEARCH LABORATORY
ATTN AMSRL WM WD
ABERDEEN PROVING GROUND MD 21005-5066

